Excitation-autoionization cross sections and rate coefficients of Cu-like ions

D. Mitnik, P. Mandelbaum, and J. L. Schwob
Racah Institute of Physics, The Hebrew University, 91904 Jerusalem, Israel

A. Bar-Shalom and J. Oreg
Nuclear Research Center—Negev, P.O. Box 9001, 84190 Beer Sheva, Israel

W. H. Goldstein
Lawrence Livermore National Laboratory, P.O. Box 808, Livermore, California 94550
(Received 23 August 1995; revised manuscript received 12 December 1995)

Detailed level-by-level calculations of the excitation-autoionization (EA) cross sections and rate coefficients were performed using the relativistic distorted-wave method along the Cu isoelectronic sequence for all the elements with $34 \leqslant Z \leqslant 92$. While in a previous work only the $3d$-$4l$ inner-shell collisional excitations had been taken into account, the present extensive calculations include the $3d^{10}4s$-$3d^{9}4snl$ ($n=4$–7 and $l=0-n-1$) and the $3p^{6}3d^{10}4s$-$3p^{5}3d^{10}4snl$ ($n=4,5$ and $l=0-n-1$) excitations. An extrapolation method is used to evaluate the contribution for higher principal quantum numbers. Configuration mixing and secondary autoionization processes following radiative decay from autoionizing levels are also included. The results show that the EA processes give a dominant contribution compared to direct ionization, up to a factor of about 15 at $Z=43$. The additional inner-shell excitations for $Z<55$ produce an increase in the EA effect varying from 20% to a factor of 2, with respect to the previously predicted $3d$-$4l$ EA rates. The additional excitations are the most significant for heavy elements with $Z>55$, since they open EA channels, resulting in an EA rate varying typically along the sequence from 3 to 1 times the direct ionization rate.

PACS number(s): 32.80.Dz, 34.80.Dp, 34.80.Kw, 52.25.Kn

I. INTRODUCTION

The understanding of the atomic processes responsible for ionization and level populating mechanisms of highly charged high-Z atoms produced in hot plasmas is very important in thermonuclear fusion diagnostics and in x-ray laser experiments. Among these, ionization by electron impact plays a central role. It has been shown, however, that excitation of inner-shell electrons into highly excited autoionizing levels followed by autoionization is an important process that can significantly enhance the total ionization rate [1–4]. The excitation-autoionization (EA) processes have now been extensively studied both theoretically and experimentally for many ions (see, for example, Ref. [5–7] and references therein). However, few EA calculations have been performed for heavy ionized atoms belonging to the sequences isoelectronic to the fourth-row elements with $3d^{10}4s^{x}4p^{y}$ ($x=1,2$ and $y=0$–6) ground state. It was shown by a study of the line emission in Ga-like rare earth ions emitted from Tokamak plasmas that such processes could be very important [8,9]. In a more recent work [10], detailed calculations of the contribution of EA through the $3d$-$4l$ inner-shell excitations were performed for ions isoelectronic to elements of the fourth row. The introduction of these data in the coronal ionization rate equations led to a significant shift in the predicted temperature of most abundance of the Kr- to Ni-like ions toward lower temperatures. Therefore, these results will have an impact on the modeling of the charge state distribution of high-Z elements in hot plasmas and in particular in x-ray laser experiments using Ni-like ions [11,12]. In the present work, more extensive level-by-level calculations of the EA processes for ions isoelectronic to Cu (ground $3d^{10}4s$) are presented. These improved calculations include now, in addition to the $3d^{9}4s4l$ configurations, the higher inner-shell excited configurations: $3d^{9}4snl$ ($n=5$–7 and $l=0-n-1$) and $3p^{5}3d^{10}4snl$ ($n=4,5$ and $l=0-n-1$). An extrapolation method is used to evaluate the contribution for higher principal quantum numbers for both $3d$-nl and $3p$-nl inner-shell excitations. Including the additional inner-shell excited configurations is of particular importance for the Cu sequence, since the main $3d^{9}4s4l$ configurations fall below the ionization limit already for $Z \geqslant 56$. Thus the present calculations allow us to extend the previous study to a higher-temperature range and also to predict an EA effect for the heavy elements ($Z \geqslant 56$). Moreover, instead of giving the rate coefficients only, we present here typical results for cross sections as well, allowing one to use the data in cases where a Maxwellian distribution of the electron velocities cannot be assumed. In addition, the present calculations take into account additional configuration interactions and also possible secondary autoionization processes following the radiative decay from the upper autoionizing levels. Finally, departure from pure coronal condition, which assumes that only the ground state is significantly populated, is discussed.

II. THEORETICAL METHODS

In the present work one assumes that the only important collisional processes are electron-impact excitation and ionization from the ground state. All other collisional processes such as collisional deexcitation or ionization from excited levels are neglected. The total cross section σ_C^{EA} for excitation autoionization from the ground configuration g ($3p^{6}3d^{10}4s$) of the Cu-like ion of a given element, to any

level k of the Ni-like ion, through inner-shell excitation of the Cu-like ion to any intermediate autoionizing level j within a given configuration or complex C is given by

$$\sigma_C^{\mathrm{EA}}(E)=\sum_{j\in C}\sigma_{gj}(E)\left[\frac{\Sigma_k A_{jk}^a+\Sigma_i A_{ji}B_i^a}{\Sigma_k A_{jk}^a+\Sigma_i A_{ji}}\right]\equiv\sum_{j\in C}\sigma_{gj}(E)B_j^a, \tag{1}$$

where $\sigma_{gj}(E)$ is the cross section for electron-impact excitation from level g to the inner-shell excited level j as a function of the incident electron kinetic energy E. A_{jk}^a is the rate coefficient for autoionization from level j to a level k of the Ni-like ion. A_{ji} is the Einstein coefficient for spontaneous emission from level j to any lower-lying Cu-like level i.

B_j^a is the *multiple* or *effective branching ratio for autoionization* from level j, defined by the term in large square brackets. This term contains in turn the effective branching ratio B_i^a for further (secondary) autoionization from level i. Thus the effective autoionization branching ratios are defined by the recursive expression

$$B_i^a\equiv\left[\frac{\Sigma_k A_{ik}^a+\Sigma_{n<i}A_{in}B_n^a}{\Sigma_k A_{ik}^a+\Sigma_{n<i}A_{in}}\right]. \tag{2}$$

This model allows one to take into account all the possible secondary autoionizations following cascading, until the radiative decay reaches a level m below the first ionization limit ($B_m^a=0$). These secondary autoionization processes were neglected in previous works [8–10].

The present level-by-level calculations have been performed following the same theoretical methods used in our previous work [10]. These are based on the HULLAC (Hebrew University Lawrence Livermore Atomic Code) computer package; this includes the computer code RELAC (Relativistic Parametric Potential Atomic Code) for atomic energy-level and radiative transition rate calculations [13], which has recently been extended to calculate the autoionization rates following the distorted-wave (DW) approximation [14]. The electron-impact excitation cross sections and rate coefficients are calculated in the DW approximation using the CROSS code [15], which is based on the factorization interpolation method.

Our calculation method does not include any resonant-excitation double-autoionization (REDA) contribution. These resonance contributions are included in the R-matrix calculations [16], as are interference effects that stem from coupling between the different channels for electron-impact excitation. This approach is more accurate than the DW method, but the need for including a large number of coupled channels can make the calculations very difficult. On the other hand, a limitation of the levels included in the expansion may reduce the accuracy of the calculations. The REDA contributions can be included in the framework of our method as independent processes, provided that channel-coupling effects were small. These effects become less and less important as the stages of ionization are higher. The DW results of Ref. [17] are in reasonably good agreement with the R-matrix calculations, demonstrating that coupling effects are small, even for the Cu-like Kr case. However, including REDA contribution would lead to extremely difficult calculations due to the large number of configurations to be included and their complex structures ($3d^9 4s4f4l$, $3d^9 4s4f5l$, $3d^9 4s5l5l'$, etc.).

In general, for plasma modeling studies, rate coefficients rather than cross sections are used. The rate coefficient S_C^{EA} for excitation-autoionization (through a given configuration C) as a function of the electron temperature T_e is given by

$$S_C^{\mathrm{EA}}=\int_0^\infty v\ f(v)\sigma_C^{\mathrm{EA}}(v)dv=\sum_{j\in C}Q_{gj}B_j^a, \tag{3}$$

where v is the electron velocity and $f(v)$ is the electron velocity distribution (assumed Maxwellian). Q_{gj} is the electron-impact excitation rate coefficient from the ground level g to level j.

The rate coefficients S^{EA} are calculated for all the elements with $34\leqslant Z\leqslant 92$ along the Cu isoelectronic sequence. The calculations are performed in the electron temperature range $0.1E_I\leqslant kT_e\leqslant 10E_I$, where E_I is the first ionization limit for each ion. The results presented here are limited to elements with $Z\geqslant 34$, since for low ionization stages the calculation method becomes less accurate.

III. CALCULATIONAL PROCEDURE

A. $3d$-nl ($4\leqslant n\leqslant 7$) inner-shell excitations

The main inner-shell collisional excitations involved in the EA processes for Cu-like ions are the $3d$-$4l$ excitations, which have been already studied in our previous work [10]. The calculations for these EA processes, as in Ref. [10], include excitations to all the levels of the $3d^9 4s4d$ and $3d^9 4s4f$ configurations, which are directly excited from the ground state ($3d^{10}4s$). The model also includes the configurations that could produce configuration mixing effects [18]: $3d^9 4p^2$ (which mixes strongly with $3d^9 4s4d$) and $3d^9 4p4d$ (which mixes with $3d^9 4s4f$). It appears, though, that the introduction of the $3d^9 4p^2$ mixing does not lead to any significant change in the EA final rates. All allowed radiative decays have been considered, i.e., transitions to the ground state and to the lower configurations $3d^{10}4l$ ($l=p,d,f$), as well as to the inner-shell excited configurations $3d^9 4s^2$ and $3d^9 4s4p$ (which lie below the first ionization limit for all the ions considered here).

The present revised calculations for $3d$-$4l$ excitations include additional configuration interactions: $3d^9 4s4d + 3d^9 4s5d$ and $3d^9 4s4f + 3d^9 4s5f$. Furthermore, in addition to the processes taken into account in the previous work, the present calculations also include the $3d$-nl ($5\leqslant n\leqslant 7$) inner-shell excitations, involving the configurations $3d^9 4snl$ ($l=0-n-1$). As will be discussed in the Sec. IV, these $3d$-nl excitations have been calculated neglecting interactions between configurations with different principal quantum numbers. For the radiative transition decays, all the relevant low-lying configurations are taken into account: $3d^{10}4s$, $3d^9 4sn'l'$ ($n'\leqslant n$ and $l'=0-n'-1$), $3d^9 4p^2$, and $3d^9 4p4d$. These include radiative transitions to lower autoionizing inner-shell excited configurations. In all the present calculations we have taken into account possible secondary autoionization processes by introducing a multiple branching ratio factor B_i^a. The autoionization processes from the $3d^9 4snl$ configurations are possible only to the ground state $3d^{10}$ of the Ni-like ions.

B. $3p$-nl (n=4,5) inner-shell excitations

The present calculations also include $3p$-nl inner-shell excitations. The $3p$-$4l$ excitations involve the $3p^5 3d^{10} 4s4l$ ($l=s,p,d,f$) configurations. The radiative transition decays considered are to the ground state ($3p^6 3d^{10} 4s$) and to the following low-lying configurations: $3p^6 3d^{10} 4l$ ($l=p,d,f$) and $3p^6 3d^9 4s4l$ ($l=s,p,d,f$). Most levels of the $3p^5 3d^{10} 4s4l$ inner-shell excited configurations lie above the first ionization limit for all the ions in the range $Z \leqslant 92$. The only exception is the configuration $3p^5 3d^{10} 4s^2$, which lies completely below the ionization limit for $Z>62$.

The $3p$-$5l$ inner-shell excitations included in our calculations are to the $3p^5 3d^{10} 4s5l$ ($l=s,p,d,f,g$) configurations. For the radiative transition decays, all the relevant low-lying configurations are taken into account: $3p^6 3d^{10} 4s$, $3p^6 3d^{10} 5l$ ($l=s,p,d,f,g$), $3p^6 3d^9 4s5l$ ($l=s,p,d,f,g$), and $3p^5 3d^{10} 4s4l$ ($l=s,p,d,f$). The model, which includes the radiative transitions to lower autoionizing levels, takes further possible autoionization from these levels into account.

The autoionization processes are mostly to the ground state $3d^{10}$ of the Ni-like ions; only for the low-Z elements ($Z<50$) is autoionization to the first excited Ni-like levels $3d^9 4s$, which lie below some Cu-like inner-shell excited levels $3p^5 3d^{10} 4snl$, possible and has been taken into account.

C. Extrapolation to higher configurations

It is difficult to undertake detailed calculations of the EA contribution for higher inner-shell configurations, since as the principal quantum number n increases, more and more levels and transitions are involved. However, the EA contribution of high configurations decreases as n increases, thus we propose the use of an approximate extrapolation method in order to evaluate all the contributions up to $n \rightarrow \infty$.

Regarding first the $3d$-nl inner-shell excitations, for low-n values ($4 \leqslant n \leqslant 7$), the results of the detailed calculations show that among all the possible excitations the dominant ones are $3d$-nd and $3d$-nf. In spite of the expected increasing number of autoionization channels for higher n, the EA contributions of the $3d$-nl excitations to levels with orbital angular momentum quantum numbers l higher than 3 are found to be negligible. This is a consequence of two contributing factors: (i) the lack of overlapping between the $3d$ and nl wave functions for $l>3$, resulting in very low collisional-strength values for the inner-shell excitations, and (ii) the rapid decrease of the autoionization rates with increasing l (the dependence of the Auger probabilities from high Rydberg states on their quantum numbers n and l is studied, for instance, in Refs. [19–21]).

Moreover, we have found an important property that can lead to a substantial reduction in the amount of calculations: for low-n numbers, the calculation results show that the ratios of the EA contribution of $3d$-nd, on the one hand, and of $3d$-nf, on the other hand, to the total $3d$-nl EA rate coefficients are almost independent of n. This result was obtained for all the elements, for $n=4$–7, and in the whole range of electron temperatures of interest. These EA contribution ratios are presented in Fig. 1. The ratios vary slightly and smoothly as a function of Z.

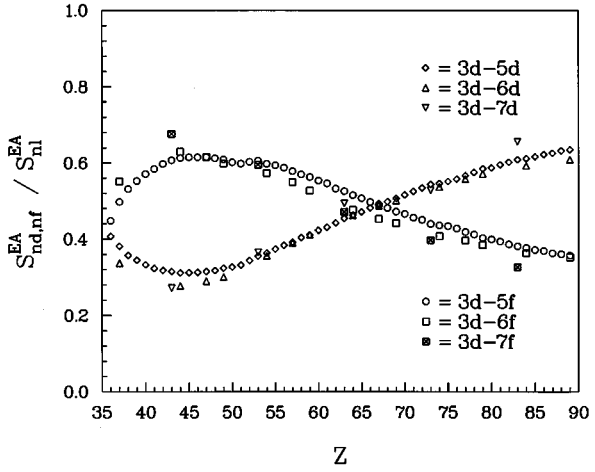

FIG. 1. Ratio of the $3d$-nd to the total $3d$-nl EA rate coefficients, and ratio of the $3d$-nf to the total $3d$-nl EA rate coefficients, for $n=5$, 6, and 7, at $kT_e=E_I$, as a function of the atomic number Z, along the Cu isoelectronic sequence.

Consequently, an analytical extrapolation only for the two excitations $3d$-nd and $3d$-nf as a function of n is needed. However, since the excitation rate coefficients of the two kinds of excitations—the $3d$-nd electric-dipole (optically) forbidden transition and the $3d$-nf electric-dipole allowed transition—behave quite differently as a function of the electron temperature, the extrapolation has to be done separately for each type of transition.

The EA rate coefficient S_C^{EA} is the sum of the product of two factors: the collisional excitation rate coefficient Q and the branching ratio for autoionization B [see expression (3)]. Therefore, in order to evaluate the asymptotic form of $S^{\mathrm{EA}}(n)$ for high quantum numbers n, it is suitable to perform the extrapolation on n independently for each factor. However, since only the relative trend of S_C^{EA} as a function of n is required, the extrapolation can be simply done for the total $3d$-nd and $3d$-nf excitation rate coefficients for the whole configurations (instead of the individual levels). Similarly, one can evaluate the configuration averaged autoionization branching ratio as a function of n.

The total $3d$-nd and $3d$-nf excitation rate coefficients have been obtained using detailed DW calculations for n up to 15. The results were introduced to get a best fit of the parameters in the Van Regemorter approximate formula [22]. Indeed, this expression is an analytical function of the temperature and of the energy levels, which can be expressed in terms of the hydrogenic asymptotic expression as a function of n. The results of this approximate extrapolation method were compared to the DW results; for $3d$-nf from $n=8$ to 15 the accuracy is found generally to be better than 10%. It should be stressed that since the sum of the contributions of the extrapolated EA rate coefficients for $n \geqslant 8$ represents less than 10% of the final total EA rates, the overall error expected is of the order of 1%.

The averaged autoionization branching ratios have been calculated for the $3d^9 4snd$ and $3d^9 4snf$ configurations from $n=4$ to 7. The results show a systematic decrease of the branching ratios along the whole isoelectronic sequence.

However, a direct extrapolation of the autoionization branching ratios on the basis of these results obtained for low-n numbers is not accurate enough. Thus the extrapolation has been done independently for the autoionization coefficients A^a and for the radiative Einstein coefficients A. The n dependence of the autoionization rate coefficients for large n is given by the well-known $(n^*)^{-3}$ behavior, where n^* is the effective principal quantum number. The hydrogenic behavior is already obtained at relatively low-n quantum numbers ($n \leqslant 10$) and therefore this approximation has been assumed for the extrapolation to higher n. On the other hand, the radiative transition rate coefficients vary asymptotically, but for these inner-shell excited levels never reach the hydrogenic behavior; the total probability of the radiative decay of the level n in the Kramers approximation gives a behavior close to n^{-5} (see, for instance, Ref. [23]). A detailed analysis of the results for up to $n=15$ enables us to obtain an asymptotic function of n and Z. The power factor obtained is less than -3. Consequently, the autoionization branching ratios decrease as a function of n (instead of the pure hydrogenic asymptotic behavior, which tends to 1).

Finally, a similar procedure has been applied in order to extrapolate the EA contributions of the $3p$-nl ($n=6$–∞) inner-shell excitations. The calculations show in this case that the dominant transitions are $3p$-np. $3p$-nd excitations, despite their high collisional strengths, do not contribute significantly to the EA rate because of the high radiative decay rates to the ground state.

IV. RESULTS

A. EA cross sections

The total electron-impact EA cross section, the direct-ionization cross section, and the total EA plus direct ionization cross section are presented in Figs. 2–6 for selected Cu-like ions: Kr^{7+}, Mo^{13+}, Xe^{25+}, Pr^{30+}, and Dy^{37+}. The direct-ionization cross section is calculated by the Lotz formula [24].

In Table I we list the main peaks in the excitation-autoionization cross-section curves for these Cu-like ions. The first column gives the inner-shell configuration transition to which the peak belongs. The second column displays the incident electron energy of the peak, i.e., the energy threshold for the excitation to the inner-shell excited level that gives the highest EA contribution within the whole configuration. The EA contribution for the *whole configuration* at this energy is given in the next column. The last column displays the value of the *total* EA cross section at the same energy.

The present results of the total EA cross section calculated for the Cu-like krypton ($Z=36$) are presented in Fig. 2, together with the energy domains of the various inner-shell transitions, indicated above the curve. The first strong increase of the EA cross section in the 130–195-eV range is due to the contributions of the $3d$-nl excitations. A further noticeable increase around 230 eV corresponds to $3p$-$4l$. In the same figure the experimental results by Bannister, Guo, and Kojima [25] have been displayed for comparison. The general trend is in fairly good agreement. In fact, a first series of calculations of the total ionization cross section without taking into account configuration interaction between configurations $3d^9 4snl$ and $3d^9 4sn'l$ with different principal quantum numbers (but the same l) leads to an overestimation of about 25–30 % with respect to the experimental values. A similar overestimation has also been noticed in theoretical results obtained by Gorczyca *et al.* [17] for Kr^{7+} using other methods. However, in that work the authors attribute the discrepancies to relaxation effects and term dependence and have reduced these discrepancies through the use of pseudo-orbitals.

Regarding the $3d$-$4d$ excitation cross sections, the main contribution comes from the excitation to the highest level $3d^9_{5/2}4s(3)4d_{5/2}[J=1/2]$ ($^2S_{1/2}$ in LS coupling). This level has a particularly strong repulsive exchange potential and therefore corresponds to a larger orbit radius than the other levels of the configuration. This level is thus poorly described by minimizing the potential parameters for the whole configuration and consequently it can cause a large error in this particular excitation cross section. As suggested by the above-mentioned authors, one way to partially correct this term dependence problem is to allow configuration mixing between the $3d^9 4s4d$ and $3d^9 4s5d$ configurations ($[4d+5d]$), so that the $4d$ orbital for the $^2S_{1/2}$ level is now represented by a weighted sum of the $4d$ and $5d$ wave functions. Thus, in the present calculations we have followed this procedure, by calculating first the $3d$-$4d$ EA cross sections including the $[4d+5d]$ configuration mixing. Then, we have included further mixed configurations $[4d+5d+6d]$, $[4d+5d+6d+7d]$, and $[4d+5d+6d+7d+8d]$ in order to obtain the asymptotic behavior of the cross section for excitation to the $^2S_{1/2}$ level. For the particular case of Kr^{7+}, the threshold value of the EA cross section asymptotically tends to 2.07 Mb. The value obtained previously (without mixing) was 3.60 Mb. By including the $[4d+5d]$ mixing only, one obtains a value of 2.17 Mb. Therefore, we conclude that, in spite of the fact that the $4d$ term dependence is not fully accounted for by using only the $[4d+5d]$ configuration interaction, this approximation can be considered accurate enough for representing the asymptotic value. This approximation is even better for higher-Z elements, in which the mixing between $4d$ and higher nd wave functions becomes smaller.

Regarding the $3d$-$5d$ excitations, including the $[4d+5d]$ mixing causes a large error in the cross-section calculations for the excitation to the $3d^9 4s5d$ configuration and especially to the dominant $^2S_{1/2}$ level. As before, in order to correct this inaccuracy, it would be necessary to include further configuration mixing with higher nd configurations. However, we have found that the previous results obtained for the $3d$-$5d$ excitations without any mixing at all with $3d^9 4snd$ configurations are close enough (better than 3% for the Kr^{7+} case) to the asymptotic values obtained by using $[4d+5d+6d+7d+8d+\cdots]$ mixing. The approximation of isolated configurations (with different n) is even more accurate for the further $3d$-nd excitations ($n>5$).

Similarly, for the $3d$-nf excitation cross sections, we have included the $[4f+5f]$ configuration mixing, but again for the $3d$-nf ($n \geqslant 5$) excitations the results obtained using the isolated configuration approximation are found to be accurate enough and are given here.

Figure 3 shows the results for the Cu-like molybdenum ($Z=42$) total EA cross section. The first step in the EA cross

TABLE I. Main contributions to the excitation-autoionization cross section, for Kr^{7+}, Mo^{13+}, Xe^{25+}, Pr^{30+}, and Dy^{37+}. The first column gives the inner-shell configuration transition to which the main EA peak belongs. The second column displays the incident electron energy threshold for the excitation to the level corresponding to the EA peak. The EA contributions for the whole configuration transition and the total EA cross section at this energy are given in the following columns.

Transition	Excitation energy (eV)	EA cross section σ_C^{EA} (cm^2)	Total EA cross section σ^{EA} (cm^2)
	(a) Kr^{7+}, E_I=124.4 eV		
$3d\rightarrow4d$	127.3	7.53[−20]	7.53[−20]
$3d\rightarrow4d$	135.1	7.84[−19]	7.84[−19]
$3d\rightarrow4d$	140.8	2.90[−18]	2.90[−18]
$3d\rightarrow4f$	155.3	1.29[−18]	4.29[−18]
$3d\rightarrow5d$	168.6	1.04[−18]	5.46[−18]
$3d\rightarrow5f$	175.7	8.98[−19]	6.30[−18]
$3d\rightarrow6d$	182.4	4.25[−19]	6.55[−18]
$3d\rightarrow6f$	186.7	4.68[−19]	6.96[−18]
$3d\rightarrow7d$	190.7	2.25[−19]	7.08[−18]
$3d\rightarrow7f$	193.6	2.89[−19]	7.29[−18]
$3p\rightarrow4p$	232.9	6.59[−19]	7.01[−18]
$3p\rightarrow5p$	285.1	1.38[−19]	6.42[−18]
	(b) Mo^{13+}, E_I=301.1 eV		
$3d\rightarrow4d$	308.6	7.90[−19]	7.90[−19]
$3d\rightarrow4f$	341.0	7.17[−19]	1.44[−18]
$3d\rightarrow4f$	345.7	8.85[−19]	1.61[−18]
$3d\rightarrow4f$	348.4	1.02[−18]	1.74[−18]
$3d\rightarrow5d$	387.8	2.46[−19]	1.90[−18]
$3d\rightarrow5f$	404.9	3.54[−19]	2.25[−18]
$3p\rightarrow4p$	420.8	2.97[−19]	2.45[−18]
$3d\rightarrow6d$	428.6	8.86[−20]	2.51[−18]
$3p\rightarrow4p$	430.0	3.43[−19]	2.56[−18]
$3d\rightarrow6f$	438.6	1.56[−19]	2.68[−18]
$3d\rightarrow7d$	447.9	4.46[−20]	2.70[−18]
$3d\rightarrow7f$	454.2	8.51[−20]	2.76[−18]
$3p\rightarrow5p$	543.4	6.15[−20]	2.26[−18]
	(c) Xe^{25+}, E_I=855.7 eV		
$3d\rightarrow4f$	855.8	6.10[−20]	6.10[−20]
$3d\rightarrow4f$	866.8	1.52[−19]	1.52[−19]
$3p\rightarrow4p$	923.9	4.08[−20]	1.90[−19]
$3p\rightarrow4p$	962.2	7.46[−20]	2.22[−19]
$3d\rightarrow5d$	1038.5	3.26[−20]	2.55[−19]
$3d\rightarrow5f$	1076.9	2.56[−20]	2.77[−19]
$3d\rightarrow6d$	1167.7	1.20[−20]	2.86[−19]
$3d\rightarrow6f$	1189.3	1.53[−20]	3.06[−19]
$3d\rightarrow7f$	1260.9	6.52[−21]	3.08[−19]
$3p\rightarrow5p$	1302.2	1.17[−20]	3.07[−19]
	(d) Pr^{30+}, E_I=1168.0 eV		
$3p\rightarrow4p$	1194.8	2.68[−20]	2.72[−20]
$3p\rightarrow4p$	1256.2	4.59[−20]	4.63[−20]
$3d\rightarrow5d$	1394.1	1.86[−20]	6.56[−20]
$3d\rightarrow5f$	1441.8	1.80[−20]	8.45[−20]
$3d\rightarrow6d$	1582.7	6.01[−21]	8.65[−20]
$3d\rightarrow6f$	1609.4	6.02[−21]	9.16[−20]
$3p\rightarrow5p$	1622.4	4.71[−21]	9.57[−20]
$3d\rightarrow7d$	1694.5	2.73[−21]	9.70[−20]

TABLE I. (*Continued*).

Transition	Excitation energy (eV)	EA cross section σ_C^{EA} (cm^2)	Total EA cross section σ^{EA} (cm^2)
	(e) Dy^{37+}, E_I=1690.5 eV		
$3p \rightarrow 4p$	1743.0	1.01[−20]	1.04[−20]
$3d \rightarrow 5d$	1977.9	8.96[−21]	2.03[−20]
$3d \rightarrow 5f$	2003.0	3.08[−21]	2.32[−20]
$3d \rightarrow 5f$	2039.5	7.31[−21]	2.72[−20]
$3p \rightarrow 5p$	2244.1	2.49[−21]	2.97[−20]
$3d \rightarrow 6d$	2256.9	2.80[−21]	3.21[−20]
$3d \rightarrow 6f$	2291.1	2.07[−21]	3.27[−20]
$3p \rightarrow 5p$	2391.3	3.37[−21]	3.37[−20]
$3d \rightarrow 7d$	2421.8	1.21[−21]	3.46[−20]

section occurs at 312 eV and is due to excitation from the ground state to the highest energy level belonging to the $3d^9 4s4d$ configuration, which is just above the ionization limit. The next increase observed in the range 335–350 eV is produced by the excitations through the $3d$-$4f$ channels. A further small step occurs around 390 eV, due to the $3d$-$5d$ inner-shell excitations, followed by a larger increase at 405 eV due to $3d$-$5f$. Some excitations of this last channel are superimposed with excitations of the type $3p$-$4p$, occurring in the energy range 395–430 eV. A few small features can still be observed at higher energies mostly produced by the $3d$-$6d$ and $3d$-$6f$ excitations. The other channels give a rather small contribution to the total EA cross section.

Figure 4 shows the results for the Cu-like xenon (Z=54). For this ion, the $3d^9 4s4d$ inner-shell excited levels lie completely below the ionization limit and, consequently, the respective EA channels are closed. The first EA strong step in the cross section is produced around 860 eV by the $3d$-$4f$ excitations. The next increases at around 920 and 960 eV are produced via the $3p$-$4p$ excitations. Some smaller enhancements can be observed at higher energies, belonging to the further transitions.

The results for the Cu-like praseodymium (Z=59) are shown in Fig. 5. In this case, no autoionization channels via $3d$-$4l$ are possible. The first two steps observed around 1195 and 1255 eV are produced via $3p$-$4p$ excitations. The $3d$-$5d$ excitations produce the two steps observed around 1370 and 1395 eV and the two increases occurring around 1420 and 1440 eV are due to $3d$-$5f$. The $3d$-$6d$ excitations are responsible for the small peaks in the range 1580–1620 eV.

Figure 6 displays the results for the Cu-like dysprosium (Z=66). The $3p^5 3d^{10} 4s4p$ inner-shell excited levels lie partially below the ionization limit. They are responsible for the peak noticeable at 1743 eV. The two increases occurring around 1940 and 1980 eV are due to the $3d$-$5d$ excitations and the next two at around 2000 and 2040 eV to $3d$-$5f$. Further steps are observed at higher energies, especially between 2240 and 2260 eV due to $3d$-$6d$.

B. Total EA rate coefficients

The total excitation-autoionization rate coefficients S^{EA}, computed by level-by-level calculations involving 872 inner-shell excited levels corresponding to the excitations $3d$-$4l$, $3p$-$4l$, $3d$-$5l$, $3d$-$6l$, $3d$-$7l$, and $3p$-$5l$, and including the extrapolated EA contributions for higher n numbers, are

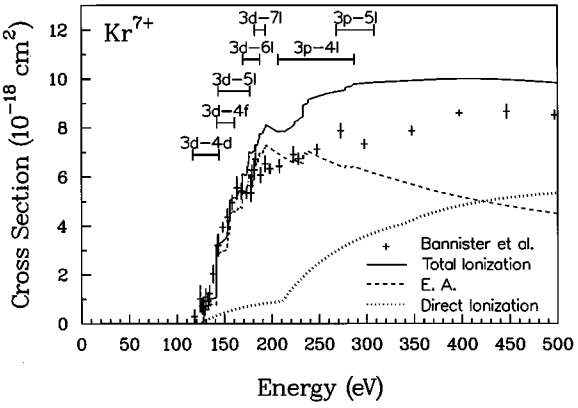

FIG. 2. Calculated direct-ionization cross section, total EA cross section, and total EA plus direct ionization cross section as a function of the incident electron energy, for Kr^{7+} ion. The energy domains of the various inner-shell transitions are indicated above the curves. Experimental results given by Bannister, Guo, and Kojima [25] are also displayed.

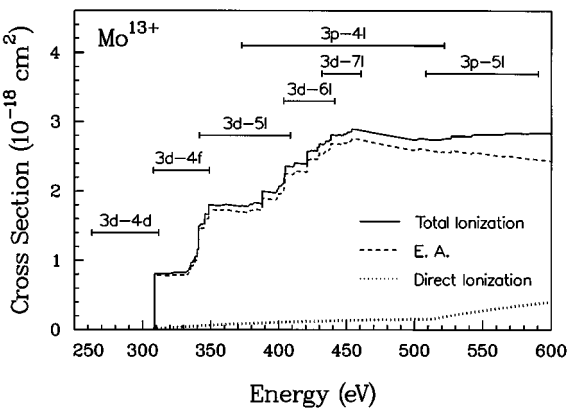

FIG. 3. Calculated direct-ionization cross section, total EA cross section, and total EA plus direct ionization cross section, for the Mo^{13+} ion. The energy domains of the various inner-shell transitions are indicated above the curves.

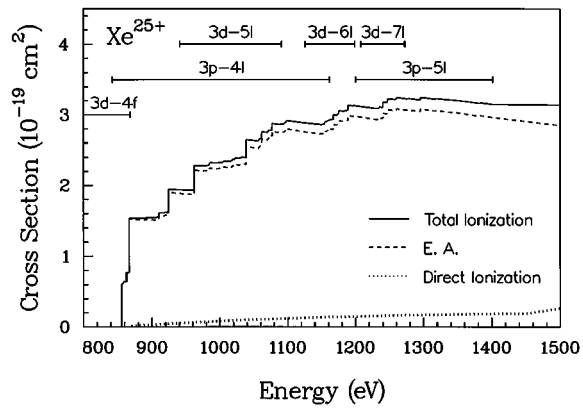

FIG. 4. Calculated direct-ionization cross section, total EA cross section, and total EA plus direct ionization cross section, for the Xe^{25+} ion. The energy domains of the various inner-shell transitions are indicated above the curves.

given in Table II. The results are presented for all the elements ($34 \leqslant Z \leqslant 92$), in a wide temperature range $0.1E_I \leqslant kT_e \leqslant 10E_I$.

In order to appreciate the contribution to the ionization enhancement given by the various EA channels, the ratio between S_C^{EA} for the configuration transitions and the direct ionization rate coefficient S (at $kT_e = E_I$) are shown in Figs. 7 and 8, together with the ratio between the *total* EA rate coefficient S^{EA} and S. Codes for quantum-mechanical calculations of the direct ionization rates with comparable accuracy to our collisional excitation rates are discussed, for instance, in Ref. [5]. However, for simplicity we have used the widely applied analytical Lotz formula [24] here since, in view of the dominant EA contribution obtained in the Cu sequence, this formula is sufficiently accurate.

For elements having $Z \leqslant 55$ the most important contribution to EA is through $3d$-$4d$ and $3d$-$4f$ inner-shell excitations (Fig. 7). At low Z, the autoionizing configurations $3d^9 4s4d$ and $3d^9 4s4f$ are relatively high with respect to the first ionization limit. For $40 \leqslant Z \leqslant 43$ the ratio S^{EA}/S increases as a function of Z. This is due to the fact that the energies of the $3d^9 4s4d$ and $3d^9 4s4f$ autoionizing levels decrease progressively as Z increases, thus favoring the inner-shell excitation processes more and more. The first abrupt decrease in S^{EA}/S occurs at $Z=44$ and has the following explanation: about 75% of the total excitation rate coefficients from the ground state to the $3d^9 4s4d$ configuration is due to excitation to a single level $3d_{5/2}^9 4s(3)4d_{5/2}[J=1/2]$. This level, which is the highest in the configuration, falls below the ionization limit for elements with Z greater than 43 (not 44, as obtained in a previous work [10], in which we did not introduce the mixing between $3d^9 4s4d$ and $3d^9 4s5d$ configurations). Consequently, the effective closing of the $3d^9 4s4d$ autoionization channels appears in this isoelectronic sequence at $Z=44$. The inner-shell transitions from the ground state to the $3d^9 4s4f$ configuration are dominated by a few levels; thus one observes the successive closing of the autoionization channels as Z further increases up to $Z=56$, for which the $3d^9 4s4f$ channels are completely closed.

The next important contributions are given by $3p$-$4l$ and $3d$-$5l$ inner-shell excitations, which have a particular importance in ions having $Z \geqslant 56$. Among the first group, the dominant transition is $3p$-$4p$ (Fig. 8), which gives a maximum EA contribution at $Z=60$; then a noticeable drop occurs at $Z=62$ and this EA channel is almost completely closed at $Z=75$. The rest of the $3p$-$4l$ inner-shell excited autoionizing levels give a S_C^{EA} rate coefficient (at $kT_e = E_I$), which is less than 10% of the direct ionization rates S in the isoelectronic sequence. Except for the $3p^5 3d^{10} 4s^2$ configuration, which lies below the ionization limit for $Z>62$, all the $3p^5 3d^{10} 4s4l$ inner-shell excited configurations still have a few levels lying above the first ionization limit for all the ions ($Z \leqslant 92$). However, their contribution to the ionization enhancement becomes negligible for elements with $Z>82$.

The contribution of $3d$-$5l$ transitions to the total ionization rates is shown in Fig. 7. The ratio S_C^{EA}/S increases from 0.4 to 0.7 up to $Z=45$, followed by a smooth decrease for higher-Z elements. This decrease is a consequence of the progressive decrease of the autoionization branching ratios, due to the increase of the radiative transition coefficients. All the $3d^9 4s5l$ configurations lie above the ionization limit for all the elements.

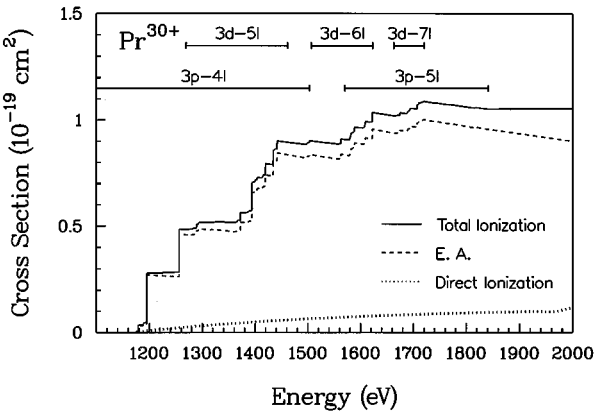

FIG. 5. Calculated direct-ionization cross section, total EA cross section, and total EA plus direct ionization cross section, for the Pr^{30+} ion. The energy domains of the various inner-shell transitions are indicated above the curves.

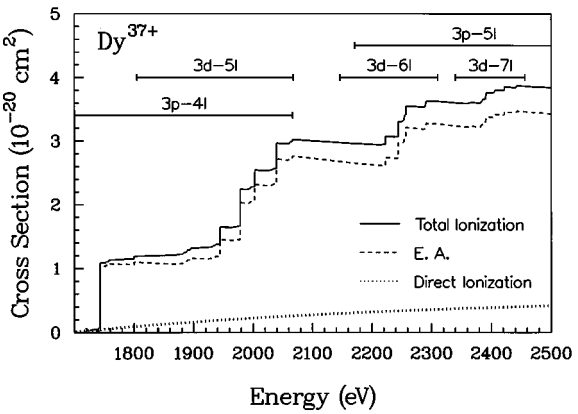

FIG. 6. Calculated direct-ionization cross section, total EA cross section, and total EA plus direct ionization cross section, for the Dy^{37+} ion. The energy domains of the various inner-shell transitions are indicated above the curves.

TABLE II. Total rate coefficients S^{EA} for excitation-autoionization through $3d^{10}4s$-$3d^{9}4snl$ and $3p^{6}3d^{10}4s$-$3p^{5}3d^{10}4snl$ inner-shell excitations in the Cu isoelectronic sequence. The rates have been calculated level by level for the $3d$-$4l$, $3d$-$5l$, $3d$-$6l$, $3d$-$7l$, $3p$-$4l$, and $3p$-$5l$ inner-shell excitations. An extrapolation method has been applied for all higher quantum numbers n. The coefficients have been calculated in the electron temperature range from 0.1 to 10 times the first ionization energy E_I and are given in $cm^3\ s^{-1}$ units. $X[-Y]$ means $X\times10^{-Y}$.

		T_e						
Element	E_I (eV)	$0.1E_I$	$0.3E_I$	$0.5E_I$	$0.7E_I$	E_I	$2E_I$	$10E_I$
Se	80.6	1.21[−13]	2.62[−10]	1.19[−9]	2.22[−9]	3.51[−9]	5.61[−9]	5.15[−9]
Br	101.6	1.39[−13]	2.57[−10]	1.14[−9]	2.12[−9]	3.32[−9]	5.25[−9]	4.94[−9]
Kr	124.4	1.68[−13]	2.52[−10]	1.09[−9]	2.02[−9]	3.14[−9]	4.91[−9]	4.68[−9]
Rb	149.2	1.73[−13]	2.41[−10]	1.03[−9]	1.89[−9]	2.92[−9]	4.53[−9]	4.34[−9]
Sr	175.9	1.66[−13]	2.21[−10]	9.38[−10]	1.71[−9]	2.63[−9]	4.08[−9]	3.92[−9]
Y	204.3	1.60[−13]	2.07[−10]	8.65[−10]	1.57[−9]	2.40[−9]	3.71[−9]	3.60[−9]
Zr	234.8	1.64[−13]	1.96[−10]	8.05[−10]	1.45[−9]	2.20[−9]	3.38[−9]	3.27[−9]
Nb	266.9	1.64[−13]	1.83[−10]	7.40[−10]	1.32[−9]	1.99[−9]	3.05[−9]	2.96[−9]
Mo	301.1	1.71[−13]	1.74[−10]	6.91[−10]	1.22[−9]	1.83[−9]	2.77[−9]	2.67[−9]
Tc	337.0	1.81[−13]	1.65[−10]	6.40[−10]	1.12[−9]	1.66[−9]	2.49[−9]	2.39[−9]
Ru	374.8	7.68[−14]	1.06[−10]	4.45[−10]	8.03[−10]	1.23[−9]	1.90[−9]	1.90[−9]
Rh	414.4	7.70[−14]	9.93[−11]	4.06[−10]	7.25[−10]	1.10[−9]	1.68[−9]	1.66[−9]
Pd	455.9	7.56[−14]	8.90[−11]	3.58[−10]	6.35[−10]	9.56[−10]	1.46[−9]	1.42[−9]
Ag	499.3	7.14[−14]	7.86[−11]	3.12[−10]	5.49[−10]	8.22[−10]	1.24[−9]	1.18[−9]
Cd	545.3	6.71[−14]	6.94[−11]	2.72[−10]	4.75[−10]	7.07[−10]	1.06[−9]	9.84[−10]
In	591.8	7.03[−14]	6.66[−11]	2.55[−10]	4.41[−10]	6.50[−10]	9.67[−10]	9.00[−10]
Sn	640.8	7.18[−14]	6.28[−11]	2.36[−10]	4.05[−10]	5.95[−10]	8.75[−10]	8.17[−10]
Sb	691.4	7.05[−14]	5.83[−11]	2.16[−10]	3.69[−10]	5.40[−10]	7.91[−10]	7.41[−10]
Te	744.4	6.37[−14]	5.12[−11]	1.89[−10]	3.22[−10]	4.71[−10]	6.89[−10]	6.47[−10]
I	799.4	5.87[−14]	4.56[−11]	1.67[−10]	2.86[−10]	4.16[−10]	6.09[−10]	5.80[−10]
Xe	855.7	5.62[−14]	4.17[−11]	1.51[−10]	2.57[−10]	3.73[−10]	5.42[−10]	5.16[−10]
Cs	915.0	3.36[−14]	2.82[−11]	1.06[−10]	1.81[−10]	2.64[−10]	3.83[−10]	3.37[−10]
Ba	974.6	1.40[−14]	1.66[−11]	6.60[−11]	1.16[−10]	1.70[−10]	2.46[−10]	1.83[−10]
La	1037.1	1.38[−14]	1.54[−11]	6.05[−11]	1.05[−10]	1.54[−10]	2.21[−10]	1.65[−10]
Ce	1102.0	1.40[−14]	1.43[−11]	5.52[−11]	9.55[−11]	1.40[−10]	1.99[−10]	1.48[−10]
Pr	1168.0	1.40[−14]	1.34[−11]	5.10[−11]	8.77[−11]	1.28[−10]	1.80[−10]	1.34[−10]
Nd	1237.3	1.39[−14]	1.25[−11]	4.71[−11]	8.04[−11]	1.17[−10]	1.64[−10]	1.22[−10]
Pm	1307.3	1.31[−14]	1.13[−11]	4.23[−11]	7.21[−11]	1.04[−10]	1.46[−10]	1.09[−10]
Sm	1379.2	6.47[−15]	7.39[−12]	2.96[−11]	5.21[−11]	7.68[−11]	1.11[−10]	8.36[−11]
Eu	1453.8	6.26[−15]	6.78[−12]	2.71[−11]	4.73[−11]	6.97[−11]	1.00[−10]	7.66[−11]
Gd	1531.1	6.12[−15]	6.28[−12]	2.48[−11]	4.33[−11]	6.36[−11]	9.10[−11]	6.99[−11]
Tb	1609.5	5.93[−15]	5.81[−12]	2.28[−11]	3.96[−11]	5.80[−11]	8.29[−11]	6.38[−11]
Dy	1690.5	5.73[−15]	5.40[−12]	2.10[−11]	3.64[−11]	5.32[−11]	7.56[−11]	5.85[−11]
Ho	1772.4	5.63[−15]	5.02[−12]	1.94[−11]	3.35[−11]	4.89[−11]	6.93[−11]	5.39[−11]
Er	1857.4	5.47[−15]	4.68[−12]	1.80[−11]	3.10[−11]	4.50[−11]	6.35[−11]	4.96[−11]
Tm	1944.4	5.30[−15]	4.37[−12]	1.67[−11]	2.87[−11]	4.16[−11]	5.85[−11]	4.56[−11]
Yb	2034.2	5.13[−15]	4.07[−12]	1.54[−11]	2.64[−11]	3.83[−11]	5.37[−11]	4.23[−11]
Lu	2125.1	5.01[−15]	3.81[−12]	1.44[−11]	2.46[−11]	3.55[−11]	4.97[−11]	3.92[−11]
Hf	2219.0	4.84[−15]	3.54[−12]	1.33[−11]	2.26[−11]	3.26[−11]	4.53[−11]	3.62[−11]
Ta	2315.4	4.69[−15]	3.33[−12]	1.24[−11]	2.11[−11]	3.04[−11]	4.22[−11]	3.36[−11]
W	2413.6	4.55[−15]	3.17[−12]	1.18[−11]	2.00[−11]	2.87[−11]	3.97[−11]	3.12[−11]
Re	2514.0	2.66[−15]	2.01[−12]	8.09[−12]	1.42[−11]	2.09[−11]	2.99[−11]	2.55[−11]
Os	2616.4	1.15[−15]	1.85[−12]	7.45[−12]	1.31[−11]	1.93[−11]	2.76[−11]	2.24[−11]
Ir	2721.9	1.02[−15]	1.63[−12]	6.63[−12]	1.16[−11]	1.72[−11]	2.46[−11]	2.06[−11]
Pt	2828.7	9.71[−16]	1.64[−12]	6.56[−12]	1.15[−11]	1.68[−11]	2.40[−11]	1.93[−11]
Au	2938.5	9.39[−16]	1.58[−12]	6.26[−12]	1.09[−11]	1.59[−11]	2.27[−11]	1.80[−11]
Hg	3051.6	9.07[−16]	1.54[−12]	6.03[−12]	1.04[−11]	1.52[−11]	2.16[−11]	1.69[−11]
Tl	3166.1	9.19[−16]	1.50[−12]	5.79[−12]	1.00[−11]	1.45[−11]	2.05[−11]	1.59[−11]
Pb	3283.4	8.70[−16]	1.43[−12]	5.50[−12]	9.48[−12]	1.38[−11]	1.94[−11]	1.48[−11]

TABLE II. (*Continued*).

		T_e						
Element	E_I (eV)	$0.1E_I$	$0.3E_I$	$0.5E_I$	$0.7E_I$	E_I	$2E_I$	$10E_I$
Bi	3403.0	8.54[−16]	1.13[−12]	4.49[−12]	7.82[−12]	1.14[−11]	1.62[−11]	1.39[−11]
Po	3525.0	8.03[−16]	1.08[−12]	4.25[−12]	7.39[−12]	1.08[−11]	1.52[−11]	1.31[−11]
At	3650.4	7.80[−16]	1.02[−12]	4.01[−12]	6.97[−12]	1.01[−11]	1.43[−11]	1.24[−11]
Rn	3777.9	7.74[−16]	9.72[−13]	3.80[−12]	6.58[−12]	9.55[−12]	1.34[−11]	1.16[−11]
Fr	3908.1	7.54[−16]	9.26[−13]	3.60[−12]	6.21[−12]	9.02[−12]	1.26[−11]	1.10[−11]
Ra	4040.6	7.43[−16]	8.81[−13]	3.41[−12]	5.86[−12]	8.50[−12]	1.19[−11]	1.04[−11]
Ac	4176.9	7.28[−16]	8.41[−13]	3.24[−12]	5.55[−12]	8.03[−12]	1.12[−11]	9.82[−12]
Th	4315.2	7.08[−16]	8.03[−13]	3.07[−12]	5.25[−12]	7.59[−12]	1.06[−11]	9.27[−12]
Pa	4455.5	6.95[−16]	7.64[−13]	2.90[−12]	4.97[−12]	7.15[−12]	9.98[−12]	8.71[−12]
U	4600.9	6.87[−16]	7.27[−13]	2.75[−12]	4.68[−12]	6.73[−12]	9.38[−12]	8.24[−12]

The contributions of $3d$-$6l$ and $3d$-$7l$ are also displayed in Fig. 7, together with the total contribution from all the $3d$-nl ($n>7$) channels. The total contribution of the extrapolated high-n channels is equal to or smaller than that given by the $3d$-$6l$ channels.

The $3p$-$5l$ inner-shell excitations involve high-energy levels and give a low contribution to the total EA rate (Fig. 8). This EA channel is dominated by the $3p$-$5p$ inner-shell excitations. All the $3p$-nl EA channels for $n>5$ give a total contribution similar to this channel along the whole isoelectronic sequence.

In order to emphasize the effect of EA on the ionization processes in plasma, it is convenient to introduce an effective enhancement factor of the collisional ionization rate coefficient due to the EA processes, defined in our previous work [10],

$$R^{\mathrm{EA}} \equiv \frac{(S+S^{\mathrm{EA}})}{S}. \tag{4}$$

The ionization enhancement factor R^{EA} is shown in Fig. 9 for three temperatures $kT_e=0.3E_I$, $0.5E_I$, and E_I. The present results show that the contribution of the EA processes is very large; for $Z=43$ at $kT_e=0.3E_I$ (which approximately corresponds to $T_{\max}$, the temperature of maximum Cu-like ion abundance in the coronal model [10]) R^{EA} reaches a value as high as 17. For comparison with our previous results [10], the ratio R^{EA} obtained taking into account only the $3d$-$4l$ inner-shell excitations is also shown, for $kT_e=0.5E_I$. For elements with $Z<44$, the contribution of the additional autoionizing configurations causes the R^{EA} factor to increase by about 20%. For elements in the $44\leqslant Z\leqslant 54$ range ($kT_{\max}\approx 0.5E_I$), the R^{EA} factor is almost twice the value obtained for the $3d$-$4l$ channels only. However, the present calculations are the most important for elements with $Z>55$, since in this case the channels $3d$-$4l$ are completely closed. In this range, the R^{EA} factor due to the other EA channels varies from about 4 for $Z=56$ ($kT_{\max}\approx 0.7E_I$) to 2 or less for the high-Z domain at the temperatures of interest ($kT_{\max}\geqslant E_I$). The relative signifi-

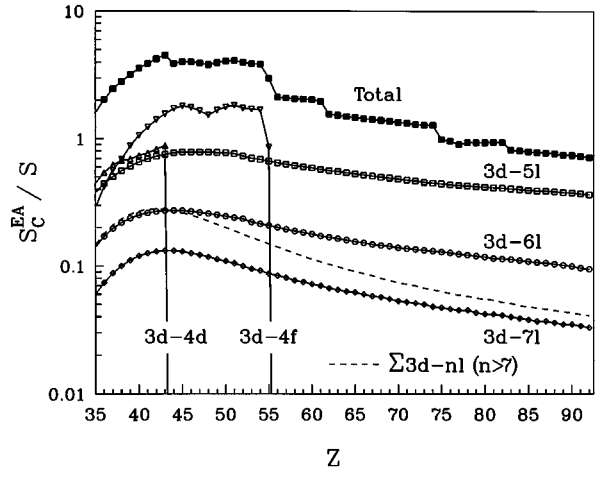

FIG. 7. Ratio of the excitation-autoionization rate coefficient S_C^{EA} to the direct ionization rate coefficient S for the $3d$-$4d$, $3d$-$4f$, $3d$-$5l$, $3d$-$6l$, $3d$-$7l$, and $\Sigma 3d$-nl ($n>7$) inner-shell excitations, at electron temperature equal to the first ionization energy E_I, as a function of the atomic number Z, along the Cu isoelectronic sequence. The ratio of the total S^{EA} rate coefficient to S is also displayed.

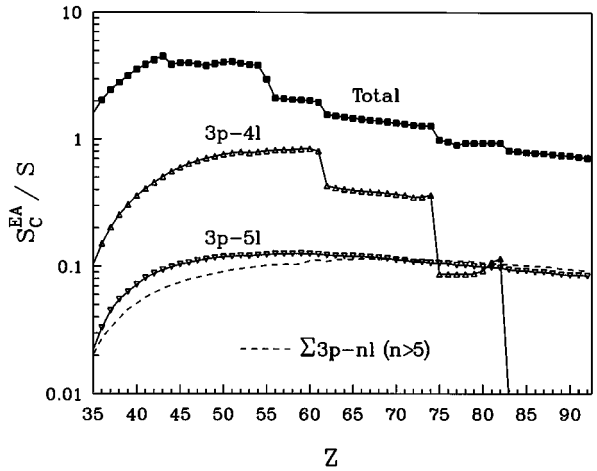

FIG. 8. Ratio of the excitation-autoionization rate coefficient S_C^{EA} to the direct ionization rate coefficient S for the $3p$-$4l$, $3p$-$5l$, and $\Sigma 3p$-nl ($n>5$) inner-shell excitations, at electron temperature equal to the first ionization energy E_I, as a function of the atomic number Z, along the Cu isoelectronic sequence. The ratio of the total S^{EA} rate coefficient to S is also displayed.

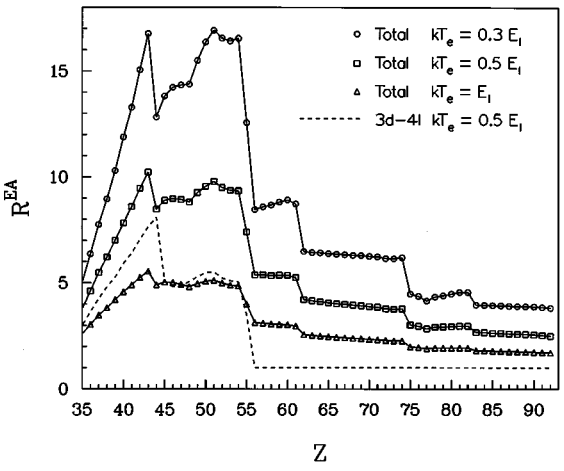

FIG. 9. Ratio R^{EA} of the total ionization rate coefficient $S^{\mathrm{EA}}+S$ to the direct ionization rate coefficient S, at electron temperatures equal to 0.3, 0.5, and 1 times the first ionization energy E_I, as a function of the atomic number Z, along the Cu isoelectronic sequence. For comparison, the ratio R^{EA} obtained by taking into account only the $3d$-$4l$ inner-shell excitations is also shown at $kT_e=0.5E_I$.

cance of the additional channels is expected to decrease for the following isoelectronic sequences (Zn- to Kr-like).

The introduction of the multiple autoionization branching ratio model in the calculations has an influence of less than 2% and only in the $45\leqslant Z\leqslant 60$ range. Outside this range, the approximate model assuming $B_i^a=0$ [in expression (1)] is in fact equivalent to the present full model. Another approximate model, in which $B_i^a=1$, would lead to an overestimate of the R enhancement factor by about 20% for low-Z values and up to 75% for high-Z elements (due to the fast increase of the radiative decay rates as the ion charge increases).

C. Density range validity of the model

Finally, a collisional-radiative model [26] assuming an optically thin plasma, which includes all the $3d^{10}4l$ levels, was used for calculating the population of the low-lying levels along the whole isoelectronic sequence, in order to define the electron density range of validity of the present calculations in which one assumes collisional excitation from the ground state only. In the coronal model conditions, indeed, only the ground state is significantly populated. However, at higher electron densities ionization (direct and EA) from other configurations must also be taken into account. For a wide temperature range, we have calculated the density at which the first excited levels ($3d^{10}4p$) have a population equal, for instance, to 10% of the ground-state population. For $Z=40$, this occurs at $N_e=3.2\times10^{16}$ cm^{-3}, for $Z=60$ at $N_e=1.5\times10^{18}$ cm^{-3}, and for $Z=90$ at $N_e=4.1\times10^{19}$ cm^{-3}.

V. CONCLUSIONS

The present work emphasizes the significant EA contribution to ionization processes in the Cu isoelectronic sequence. Detailed calculations using the relativistic parameter potential and the distorted-wave method were performed, enabling level-by-level computations of the EA cross sections and rate coefficients through the most important inner-shell excitations, which are the $3d$-nl ($n=4$–7) and $3p$-nl ($n=4,5$) transitions. These computations have been done for all the elements in the range $34\leqslant Z\leqslant 92$, along the isoelectronic sequence. These computations also include the main configuration interactions, radiative transitions among autoionizing levels, and further possible autoionization from these levels. It is worth noting, based on the present results, that the usual approach in which these further autoionizations are ignored ($B_i^a=0$) is quite accurate. Extrapolations for the $3d$-nl ($n>7$) and $3p$-nl ($n>5$) excitations were also included, leading to a contribution to the total EA rates varying from about 5% to 20% as Z increases along the sequence.

Result of the computation of EA cross sections are presented for selected Cu-like ions: Kr^{7+}, Mo^{13+}, Xe^{25+}, Pr^{30+}, and Dy^{37+}. In some cases, the enhancement in the ionization cross section due to EA processes is larger by more than one order of magnitude, in a wide range of the incident electron energy.

The results of the present calculations in the Cu sequence predict that the EA processes increase the total ionization rate by a very large factor, which varies from 5 to 17 in the $35\leqslant Z\leqslant 43$ range (for $kT_e\approx 0.3E_I$). This factor is around 9 in the $44\leqslant Z\leqslant 54$ range (for $kT_e\approx 0.5E_I$) and decreases from about 4 to less than 2 for the heavier elements in the $56\leqslant Z\leqslant 92$ range at the relevant temperatures ($kT_e\approx E_I$). These results show the importance of the EA effect in the fractional ion abundance modeling as a function of T_e in hot plasmas, such as in tokamaks, predicting a significant decrease in the temperature of maximum abundance, even larger than that calculated in our previous work [10].

[1] B. Peart and K. Dolder, J. Phys. B **1**, 872 (1968); **8**, 56 (1975).
[2] J. W. Allen and A. K. Dupree, Astrophys. J. **155**, 27 (1969).
[3] R. D. Cowan and J. B. Mann, Astrophys. J. **232**, 940 (1979).
[4] D. H. Crandall, R. A. Phaneuf, D. C. Gregory, A. M. Howald, D. W. Mueller, T. J. Morgan, G. H. Dunn, D. C. Griffin, and R. J. W. Henry, Phys. Rev. A **34**, 1757 (1986).
[5] *Electron Impact Ionization*, edited by T. D. Märk and G. H. Dunn (Springer-Verlag, New York, 1985).
[6] K. Dolder, Adv. At. Mol. Opt. Phys. **32**, 69 (1994).
[7] D. L. Moores and K. J. Reed, Adv. At. Mol. Opt. Phys. **34**, 301 (1995).
[8] P. Mandelbaum, M. Finkenthal, E. Meroz, J. L. Schwob, J. Oreg, W. H. Goldstein, M. Klapisch, L. Osterheld, A. Bar-Shalom, S. Lippman, L. K. Huang, and H. W. Moos, Phys. Rev. A **42**, 4412 (1990).
[9] J. Oreg, W. H. Goldstein, P. Mandelbaum, D. Mitnik, E. Meroz, J. L. Schwob, and A. Bar-Shalom, Phys. Rev. A **44**, 1741 (1991).

[10] D. Mitnik, P. Mandelbaum, J. L. Schwob, J. Oreg, A. Bar-Shalom, and W. H. Goldstein, Phys. Rev. A **50**, 4911 (1994).
[11] S. Maxon, P. Hagelstein, J. Scofield, and Y. Lee, J. Appl. Phys. **59**, 294 (1986).
[12] S. R. Elliot, P. Beiersdorfer, and J. Nilsen, Phys. Rev. A **51**, 1683 (1995).
[13] M. Klapisch, J. L. Schwob, B. Fraenkel, and J. Oreg, J. Opt Soc. Am. **67**, 148 (1977).
[14] J. Oreg, W. H. Goldstein, M. Klapisch, and A. Bar-Shalom, Phys. Rev. A **44**, 1750 (1991).
[15] A. Bar-Shalom, M. Klapisch, and J. Oreg, Phys. Rev. A **38**, 1733 (1988).
[16] P. G. Burke and W. D. Robb, Adv. At. Mol. Phys. **11**, 143 (1975).
[17] T. W. Gorczyca, M. S. Pindzola, N. R. Badnell, and D. C. Griffin, Phys. Rev. A **49**, 4682 (1994).
[18] P. Mandelbaum, J. F. Seely, A. Bar-Shalom, and M. Klapisch, Phys. Rev. A **44**, 5744 (1991).
[19] W. E. Cooke and T. F. Gallagher, Phys. Rev. A **19**, 2151 (1979); R. R. Jones and T. F. Gallagher, *ibid*. **38**, 2846 (1988).
[20] J. N. Gau and Y. Hahn, Phys. Lett. **68A**, 197 (1978).
[21] S. I. Nikitin and V. N. Ostrovsky, J. Phys. B **13**, 1961 (1980).
[22] H. Van Regemorter, Astrophys. J. **136**, 906 (1962).
[23] Y. B. Zel'dovich and Y. P. Raizer, *Physics of Shock Waves and High-Temperature Hydrodynamic Phenomena* (Academic, New York, 1966), Vol. I, p. 300.
[24] W. Lotz, Z. Phys. **206**, 205 (1967); **216**, 241 (1968); **232**, 101 (1970).
[25] M. E. Bannister, X. Q. Guo, and T. M. Kojima, Phys. Rev. A **49**, 4676 (1994).
[26] D. R. Bates, F. R. S. Kingston, and R. W. P. McWhirter, Proc. R. Soc. London Ser. A **267**, 297 (1962).